RSC Advances

PAPER

View Article Online
View Journal | View Issue

Check for updates

Cite this: *RSC Adv.*, 2017, **7**, 38998

Biofunctionalized zinc peroxide (ZnO_2) nanoparticles as active oxygen sources and antibacterial agents†

Christian Bergs,[a] Lisa Brück,[a] Ruben R. Rosencrantz,[b] Georg Conrads,[c] Lothar Elling[b] and Andrij Pich*[a]

Oxygen is one of the most important substances for physiological reactions and metabolisms in biological systems. Through the tailored design of oxygen-releasing materials it might be possible to control different biological processes. In this work we synthesized for the first time zinc peroxide nanoparticles with controlled sizes and biofunctionalized surfaces using a one-step reaction procedure. The zinc peroxide nanoparticles were obtained with tunable sizes (between 4.0 ± 1.2 nm and 9.4 ± 5.2 nm) and were decorated with glucose 1-phosphate (Glc-1P). The specific interaction of the phosphate function of Glc-1P with the nanoparticle surface was monitored by solid state ^{31}P-NMR and zeta-potential measurements. Furthermore, using fluorescence measurements we demonstrated that anchored glucose molecules on the nanoparticle surface are accessible for specific interactions with lectins. It could be shown that these interactions strongly depend on the amount of Glc-1P attached to the nanoparticle surface. Additionally it was demonstrated that the oxygen release from biofunctionalized zinc peroxide nanoparticles could be tuned according to the chemical composition of the nanoparticles and the pH of the aqueous solution. The antibacterial efficiency of the synthesized nanoparticles against *Enterococcus faecalis*, *Aggregatibacter actinomycetemcomitans*, *Porphyromonas gingivalis* and *Prevotella intermedia* was evaluated by determination of minimal bactericidal concentration (MIC).

Received 6th June 2017
Accepted 2nd August 2017

DOI: 10.1039/c7ra06332f

rsc.li/rsc-advances

Open Access Article. Published on 09 August 2017. Downloaded on 2/13/2026 8:44:47 AM.
This article is licensed under a Creative Commons Attribution 3.0 Unported Licence.

1 Introduction

The majority of bacterial infections are treated through antibiotics these days. These drugs are essential in many medical treatments like chemotherapy, organ transplantation and surgical procedures and reduce the human mortality and morbidity drastically.[1,2] However, the number of antibiotic resistant microorganisms is increasing globally. This resistance can occur through intrinsic effects, mutations in chromosomal genes or horizontal gene transfers.[3] For example bacteria can reduce their cell wall permeability, which causes a drug concentration reduction inside the bacterial cells and reduction of drug efficiency.[4,5] Furthermore Gram-negative and -positive bacteria posses transport proteins (efflux pumps (EP)) in the cytoplasmic membrane, which can remove toxic molecules.[5,6] Another mechanism which increases bacterial resistance is the destruction of the active components of antibiotics.[1,7] Further the formation of bacterial biofilms represents a highly effective protection method against antibiotics.[8] The biofilm itself acts as a diffusion barrier and neutralizer, against antibiotics which minimizes the intracellular antibiotic concentration.[9–13] Additionally the bacterial mutation rates and horizontal gene transmissions are significantly higher in biofilms compared to planktonic bacterial cells, which causes further antibiotic resistances.[13,14]

Therefore there exists a tremendous need in development of new highly efficient antibacterial substances. For example antimicrobial peptides which can disrupt the bacteria cell wall causing leakage of the cellular content were tested on mammalian cells.[15] Further antisense oligonucleotides were used to influence the gene expression directly at the RNA. The nucleotides consist typically of 10–30 residues, which are complementary to the mRNA of interest. Thereby the nucleotides can block genes which are essential for the survival of the bacteria.[16,17] Also different antibacterial polymers were developed and tested. Poly(hexamethylene biguanide) (polyhexanide) showed antibacterial properties against Gram-positive and -negative bacteria. The antibacterial activity of this cationic polymer is based on the interaction of the biguanide groups with the cytoplasmic membrane, the lipopolysaccharide and the peptidoglycan of the bacterial cell wall resulting in

[a]*DWI-Leibniz Institute for Interactive Materials e.V., Institute of Technical and Macromolecular Chemistry, RWTH Aachen University, Aachen, Germany. E-mail: pich@dwi.rwth-aachen.de*

[b]*Laboratory for Biomaterials, Helmholtz-Institute for Biomedical Engineering, RWTH Aachen University, Aachen, Germany*

[c]*Division of Oral Microbiology and Immunology, Department of Operative and Preventive Dentistry & Periodontology, RWTH Aachen University Hospital, Aachen, Germany*

† Electronic supplementary information (ESI) available. See DOI: 10.1039/c7ra06332f

This journal is © The Royal Society of Chemistry 2017

Open Access Article. Published on 09 August 2017. Downloaded on 2/13/2026 8:44:47 AM.
This article is licensed under a Creative Commons Attribution 3.0 Unported Licence.

membrane destabilization and cellular leakage.[18] Recently, functional aqueous nanogels decorated with a controlled amount of surface-drafted antimicrobial isoeugenol molecules have been developed.[19] These nanogels showed antibacterial activity against different Gram-positive and Gram-negative pathogens and cell-adhesive as well as tissue-cell growth promoting properties.

Among inorganic antibacterial agents, silver has been used for many centuries. It is thought that silver ions bind to thiol groups (–SH) in enzymes and subsequently cause the deactivation of enzymes. Recently, silver nanoparticles with diameter of 7.1 ± 1.2 nm were synthesized *via* a protein-mediated reduction and their influence on the growth of *Escherichia coli* and *Pseudomonas aeruginosa* was investigated. It could be shown that the antibacterial properties were dependent on the nanoparticle concentration and that the interaction with the bacteria caused rupture of the cell membrane resulting in cell death.[20] Further silver nanoparticles can disrupt the cell envelope, oxidize cell components and inactivate the respiratory chain enzymes, which leads to the production of reactive oxygen species.[21–26] The immobilization of silver and iron oxide nanoparticles on a graphene oxide surface led to an antibacterial nano-composite. This material showed better antibacterial properties against *E. coli* and *Staphylococcus aureus* compared to pure silver nanoparticles, which was caused through hydrophobic domains on the graphene oxide sheets. This increased the contact between the immobilized silver nanoparticles and the bacteria leading to higher activities.[27–32] Furthermore layer-by-layer films of pure graphene oxide and poly(allylamine hydrochloride) showed also antibacterial properties against *E. coli* K12 MG1655. It was shown that these properties could be tuned by the layer numbers and by near-infrared laser irradiation. The observed activity increases were explained through increased layer roughness and synergistic effects resulting from membrane-stresses.[33] Zinc oxide nanoparticles possess antibacterial properties. Previous studies could show that the antibacterial activity increased with decreasing nanoparticle diameter and increasing nanoparticle concentrations.[34,35] Smaller particles can more easily adhere to (or even penetrate into) bacterial membranes due to their larger interfacial area, which increases the efficiency. Further it was shown that the photocatalytic generation of ROS is the major contributor to the antibacterial properties of zinc oxide nanoparticles. Zinc oxide generates electrons and holes under UV or visible light irradiation which can interact with water forming hydroxyl and/or superoxide anions which can induce bacteria cell death.[36] Another recent antibacterial approach was the synthesis of hollow mesoporous silica nanoparticles loaded with the antituberculosis drug isoniazid. Particle diameter of approximately 100.0 nm could be achieved and the antibacterial properties against *M. smegmatis* were investigated. It could be proven that the loaded nanoparticles were more effective compared to the pure drug which was explained through increased intrabacterial accumulation of isoniazid and the nonspecific adsorption of the positively charged nanoparticles on the negatively charged bacteria. This interaction led to bacteria injury, incomplete cell walls and even cell rupture and death.[37–39]

Substances capable of releasing oxygen can also act as antibacterial agents against obligate to facultative anaerobes and microaerophilic aerobes. Previous studies proved that the bacteria concentration in infected tissues decreased constantly with increasing oxygen concentration.[40–44] This observation was explained through the metabolization of oxygen into ROS species through the continuous chain reaction mode and leukocytes present in the blood. The transformation of leukocytic superoxide anions to oxygen derivatives like hydrogen peroxide, hydroxyl radicals or oxygen radicals (ROS) is highly oxygen concentration dependent and one of the most important host defenses against bacterial infections.[45] Facultative anaerobes, microaerophilic aerobes but especially obligate anaerobes lack many or even all of the antioxidant defenses like superoxide dismutase, catalase and peroxidase. Therefore ROS species can impair bacterial amino acids, disturb their metabolic substrate transport, inhibit bacterial enzymatic activities by oxidizing the sulphydryl groups of amino acids or stop the bacterial reproduction by blockage of RNA transcriptions and DNA syntheses.[46] Based on these considerations a controlled and specific oxygen release induced by chemical compounds would be of high interest for antibacterial applications. Zinc peroxide is one of these compounds (Fig. 1). Previous studies showed that zinc peroxide nanoparticles are capable of releasing oxygen triggered by temperature or pH value of the dispersion media. It could be shown that the nanoparticles released continuously oxygen for approximately 3.5 days at pH values lower 7.5 in aqueous dispersion. The amount of released oxygen was dependent and controllable by the different sample compositions and the chosen pH value.[47] The zinc peroxide nanoparticles, which could be used for biomedical applications have to fulfill two requirements: they have to be small and uniform to guarantee a homogeneous distribution and controlled oxygen release and they should be biofunctionalized to ensure a specific interaction with the biological system.

The aim of this work was to synthesize zinc peroxide nanoparticles decorated with bioactive sugar molecules and to explore their oxygen release in aqueous media, their protein binding properties as well as antibacterial properties against

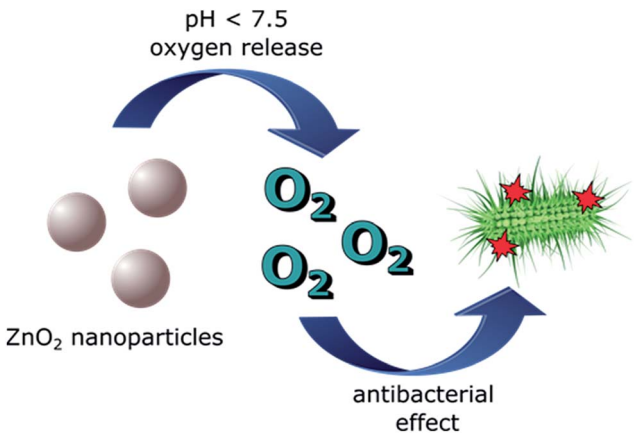

Fig. 1 Schematic illustration of oxygen release from zinc peroxide nanoparticles and the resulting antibacterial effect.

Open Access Article. Published on 09 August 2017. Downloaded on 2/13/2026 8:44:47 AM. This article is licensed under a Creative Commons Attribution 3.0 Unported Licence.

different bacteria. Especially the biofunctionalization and the detailed bioactivity investigations were never performed for zinc peroxide nanoparticles to our knowledge. Recently we showed that high pressure impinging jet reactor (MRT CR5, Microfluidics®) is best suited to obtain ultrasmall monodisperse and colloidally stable ZnO_2 nanoparticles by reaction of zinc acetate with hydrogen peroxide.[47] Classical synthesis routes like hydrothermal synthesis, laser ablation or sol gel synthesis always led to aggregation and high polydispersities of the nanoparticles which made them not suitable for biomedical applications.[48–50] The impinging jet reactor uses pressures up to 1400 bar and a y-formed reaction chamber with channel diameter of 75 μm which creates very high shear and impact forces (7×10^6 s^{-1}) inside the reaction chamber. These efficient mixing conditions in combination with stabilizing agents prevent the aggregation/agglomeration of the nanoparticles resulting in a uniform and stable product.[47] In this work we used glucose-1-phosphate (Glc-1P) for the stabilization of the ZnO_2 nanoparticles in aqueous medium and for introduction of the bioactive glucose molecules to the nanoparticle surface. The glucose functions acted as specific linker to the lectin Concanavalin A (ConA) which was proven by fluorescence measurements. The precursor : glucose-1-phosphate ratio was systematically varied to investigate its influence on the ZnO_2 nanoparticle size, amount of grafted glucose molecules and oxygen release properties.

2 Experimental

2.1 Materials

All following chemicals were purchased from Aldrich, VWR, VectorLabs and Pfeifer & Langen GmbH & Co. KG and were used without further purification: zinc acetate dihydrate (Aldrich, ≥99.0%), hydrogen peroxide (VWR, 30 wt%), glucose-1-phosphate (Pfeifer & Langen GmbH & Co. KG; purity not available), ConA (VectorLabs), Oregon Green 488 NHS-Ester (ThermoFisher Scientific) and fully demineralized water.

2.2 Synthesis of ZnO_2 nanoparticles

The synthesis was carried out in a Microfluidizer MRT CR5 of Microfluidics® (Fig. ESI1†). This device consists of an intensifier pump and a y-formed reaction chamber with channel diameter of 75 μm. The pump itself is capable of creating pressures up to 1400 bar, which results in combination with the small channels of the reaction chamber in very high shear and impact forces (7×10^6 s^{-1}) inside the reaction chamber. This impinging-jet reactor can be used as a continuous batch reactor which allows an easy control over parameters like reaction time and particle diameter by simply recycling the reaction solution. Cycle number (reaction time) experiments were performed at 10, 20, 30 and 40 cycles (4 to 16 minutes) with the following reaction solution: 1.66 g (7.61×10^{-3} mol) $Zn(ac)_2 \cdot H_2O$, 1.98 g (7.62×10^{-3} mol) Glc-1P, 7.5 mL (0.065 mol) 30 wt% H_2O_2 solution and 192.5 mL demineralized water (ZnO_2/Glc-1P (1/1) sample) (Scheme 1).

$$Zn(CH_3COO)_2 \cdot 2H_2O + H_2O_2 \xrightarrow{1400\ bar} ZnO_2 + 2\ CH_3COOH + 2H_2O$$

Scheme 1 Chemical reaction mechanism for the formation of zinc peroxide from zinc acetate dihydrate and hydrogen peroxide.

Four of these solutions were processed at the different cycle numbers and subsequent freeze dried to eliminate the water. Afterwards the resulting solid was washed three times with demineralized water and centrifuged at 14 000 rpm for 30 minutes. The washing solution was removed by decantation and the solid was dried at room temperature. We found that 30 cycles (12 minutes) was best suitable reaction time, which was kept constant for the reactions where different zinc acetate : glucose-1-phosphate ($Zn(ac)_2$: Glc-1P) ratio was varied. These experiments were performed at the same concentrations like for the ZnO_2/Glc-1P sample only the amount of the stabilizer Glc-1P was varied. The following amounts were used: 0.98 g (3.79×10^{-3} mol) Glc-1P for the ZnO_2/Glc-1P (2/1) sample, 0.47 g (1.82×10^{-3} mol) Glc-1P for the ZnO_2/Glc-1P (4/1) sample, 0.32 g (1.25×10^{-3} mol) Glc-1P for the ZnO_2/Glc-1P (6/1) sample, 0.24 g (0.95×10^{-3} mol) Glc-1P for the ZnO_2/Glc-1P (8/1) sample and 0.19 g (0.76×10^{-3} mol) Glc-1P for the ZnO_2/Glc-1P (10/1) sample. The purification steps were similar to the procedure mentioned above.

2.3 Oxygen release

The pH dependent oxygen release of the different nanoparticle samples was determined *via* long term measurements (6 to 7 days) under argon atmosphere with an optical oxygen sensor FDO®925 from WTW. This sensor can quantify the amount of dissolved oxygen in aqueous media *via* time dependent fluorescence measurements. The sealed sensor head consists of a membrane containing a fluorescent dye and a pulsed laser which generates low energy radiance (green light). The laser irradiates the fluorescent dye inside the membrane which causes the emission of longer wavelength light during its relaxation which then is measured by the sensor. When oxygen is present in the measurement solution it diffuses through the membrane and shortens the emission duration of the fluorescent dye depending on the oxygen concentration which leads to the quantification of the oxygen.[47]

2.4 Interaction of ZnO_2 nanoparticles with lectin concanavalin A

The interaction between the nanoparticles and the lectin Concanavalin A (ConA) was investigated by fluorescence measurements which were carried out on a Synergy 2 from BioTek®. The used ConA was labeled with Oregon Green 488 NHS-Ester by reacting 10 mg ConA with 3 eq. dye in phosphate–bicarbonate buffer at pH 8.3. The reaction was left in the dark overnight. Removal of residual unreacted dye was accomplished by SEC using Sephadex G-25 with PBS as mobile phase. ConA-Oregon Green was stored at 4 °C. The fluorescence measurements were carried out with excitation and emission wavelength of 485 and 528 nm, which were used for the quantifications of the immobilized ConA. The immobilization of the ConA on the

 This journal is © The Royal Society of Chemistry 2017

Open Access Article. Published on 09 August 2017. Downloaded on 2/13/2026 8:44:47 AM. This article is licensed under a Creative Commons Attribution 3.0 Unported Licence.

nanoparticle surface was done by dispersing 0.5 mg of the corresponding sample in 500 μL buffer containing 10.0 mM HEPES, 150.0 mM NaCl and 0.1 mM $CaCl_2$ followed by adding 20 μL ($c = 20$ μg mL^{-1}) of the labeled ConA. This mixture was incubated for 30 minutes and subsequently washed four times with a buffer consisting of 10.0 mM HEPES, 150.0 mM NaCl and 0.1 mM $CaCl_2$, 0.05% Tween-20 to eliminate excessive ConA. Different amounts of mannose ($c = 2.0$ g L^{-1}; 20, 40, 60, 80, 100, 120, 140, 160, 180 and 200 μL) were added to the used buffer for the inhibition measurements, while the following preparation steps were equally to the other fluorescent measurements.

2.5 Antibacterial tests

To prove antimicrobial properties of the zinc peroxide nanoparticles we selected four pathogenic bacterial species with different degrees of oxygen tolerance: (i) *Enterococcus faecalis*, a Gram-positive, facultative anaerobic species which tolerates different atmospheric conditions and is frequently isolated from a variety of infectious processes. It most commonly infect the urinary tract, bloodstream, endocardium, burn and surgical site wounds, abdomen, biliary tract, catheters and other implanted medical devices and is used as pathogenic model organism. It is generally recognized as a robust organism and can be found in the oral cavity attached to implants; (ii) *Aggregatibacter actinomycetemcomitans*, a Gram-negative, capnophilic and fastidious organism which tolerates and needs a little amount of oxygen (microaerophilic). Together with the species mentioned below it is involved in the initiation and progression of human marginal periodontitis or peri-implantitis (inflammation around teeth or titanium implants in the oral cavity); (iii) *Porphyromonas gingivalis* and (iv) *Prevotella intermedia*, both Gram-negative, obligate anaerobic rods with almost no (*P. gingivalis*) or very little (*P. intermedia*) oxygen tolerance.[51–54] The latter three species (*A. actinomycetemcomitans*, *P. gingivalis* and *P. intermedia*) were chosen because one application of zinc peroxide nanoparticles might be to form a protective layer around the subgingival part of (i) teeth, preventing periodontitis or (ii) dental implants, preventing peri-implantitis.

Zinc peroxide nanoparticles with 50.89 wt% ZnO_2 plus 49.10 wt% Glc-1P (ZnO_2/Glc-1P (2/1)_30c (12 min)) and 30.53 wt% ZnO_2 plus 69.49 wt% Glc-1P (ZnO_2/Glc-1P (1/1)_30c (12 min)) were used for the initial testing. A stock solution of 2000 μg mL^{-1} of both nanoparticles was prepared using appropriate culture media: Mueller–Hinton Broth (MHB) in the case of *E. faecalis*, Brain–Heart-Infusion Broth (BHI) in the case of the three more fastidious organisms. In the case of *P. gingivalis* and *P. intermedia* BHI was further supplemented with hemin and vitamin K1 (both Becton Dickinson, and both 2 wt% end concentration) as well as with isovitalex (Becton Dickinson, 2 v% end concentration). From these stock solutions the dilutions 1 : 2, 1 : 10, 1 : 20, 1 : 40, 1 : 80, and 1 : 160 were prepared in a 96-well-microtiterplate resulting in corresponding final concentrations of the nanoparticles of 1000 μg mL^{-1}, 200 μg mL^{-1}, 100 μg mL^{-1}, 50 μg mL^{-1}, 25 μg mL^{-1}, 12.5 μg mL^{-1} and in a total volume of 200 μL. The dilutions were prepared with culture media (see above) and pre-culture (see below). For the pre-cultures, the bacteria were grown aerobically (*E. faecalis*), in 5–10% CO_2 (*A. actinomycetemcomitans*) or anaerobically (*P. gingivalis* and *P. intermedia*) for 24–48 h at 37 °C. With each pre-culture between 10 000 and 100 000 cells were added to the microtiter wells. By this method the substance-depending minimal inhibitory concentration (MIC) was determined (Fig. 7). The minimum inhibitory concentration (MIC) is the lowest concentration of an antibacterial agent required to inhibit further growth of a particular bacterium. From every well of the microtiter plate (Fig. 7a) an aliquot of 3 μL was plated on Trypticase-Soy-Agar with 5% sheep blood (Oxoid PB5012A, Wesel, Germany) to determine the minimal bactericidal concentration (MBC, Fig. 7b). In contrast to the MIC, the minimum bactericidal concentration (MBC) is the lowest concentration of an antibacterial agent required to kill a particular bacterium.

2.6 Analytical methods

The crystal structure of the zinc peroxide nanoparticles were characterized *via* X-ray-diffraction measurements (XRD) on a PANalytical Empyrean, using a CuK_α radiation ($\lambda = 0.1542$ nm).

The sample compositions were determined *via* inductively coupled plasma atom emission spectroscopy (ICP-OES) on a Spectroflame D of the company Spectro. 1.0 mg of each sample were dispersed in 2.0 mL Milli-Q water followed by addition of 0.5 mL hydrochloric acid ($c = 1.0$ mol L^{-1}). The obtained solution was stirred for five days and afterwards measured.

The nanoparticle sizes and morphologies were determined *via* transmission electron microscopy (TEM) on a Libra 120 from Zeiss ($U = 120.0$ kV). The average sizes were determined by measuring diameters of at least 100 nanoparticles and calculating their standard deviation. One nanoparticle dispersion droplet ($c = 3.0$ g L^{-1}) was placed on 400 mesh carbon coated copper grid (EMS, USA) and dried over night for each measurement.

The surface properties of the nanoparticles and their interaction with the Glc-1P were investigated *via* pH dependent zeta potential measurements and *via* ^{31}P high resolution magic-angle sample spinning spectroscopy (^{31}P-HRMAS). High-power proton decoupled ^{31}P high-resolution magic-angle sample spinning NMR spectra were measured at 23 °C temperatures with a Bruker Avance III HD 700. The spinial64 pulse sequence was applied to proton frequency for ^{31}P–^{1}H heteronuclear decoupling and NMR spectrometer frequency for ^{31}P was 283.367 MHz. All the ^{31}P-HRMAS spectra were externally referenced to ammonium phosphate monobasic that has the ^{31}P resonance at +1 ppm relative to phosphorous acid 85% in H_2O used as zero ppm reference. The rotor frequency was 5 kHz, the recycle delay was 7 s, the radio-frequency pulse length was 4 μs (75 W), while the dwell time was 4 μs, and the number of scans was 2016. The time domain data were 4k and the zero filling was done with 16k. The relative spectral integral intensities of the peaks were measured using TopSpin 3.2 Bruker software. Zeta potential measurements were done with Malvern Zetasizer

Open Access Article. Published on 09 August 2017. Downloaded on 2/13/2026 8:44:47 AM.
This article is licensed under a Creative Commons Attribution 3.0 Unported Licence.

Nano ZS combined with an autotitrator MPT-2. The pH value of the measurement dispersion (c = 1 g L^{-1}) was automatically adjusted with hydrochloric acid and sodium hydroxide solutions (c = 1 mol L^{-1}). The measurements were performed in a pH range from 2.0 to 10.0.

3 Results and discussion

3.1 Chemical structure, size and morphology of ZnO_2 nanoparticles

The obtained zinc peroxide nanoparticles were synthesized with our recently developed continuous and fast synthesis approach (high pressure impinging-jet reactor).[47] Additionally we introduced glucose-1-phosphate as stabilizing and functionalization agent for the first time and investigated the influence of different reaction times/cycle numbers (4 to 16 min) and precursor : glucose-1-phosphate ratios (1/1, 2/1, 4/1, 6/1, 8/1, 10/1) on the nanoparticle properties systematically. XRD measurements showed the typical reflexes for the cubic crystal structure of zinc peroxide at 2θ = 31.0, 36.5, 53.0 and 63.0° (indexes: 111, 200, 220 and 311) for all synthesized nanoparticles, whereby only one representative measurement is shown in Fig. 2 (other measurements see ESI2†). Further broadened reflexes could be detected for all samples indicating the presence of nanoparticles.[55] By measuring the full width at half maximum (FWHM) of the reflexes 220 and 311 it was possible to calculate the crystallite sizes of the different samples *via* the well known Debye Scherrer equation (see ESI3†). Values between 2.7 ± 0.2 and 3.3 ± 0.5 nm could be calculated which supported the nanoparticle diameter determinations based on TEM measurements (see discussion below).

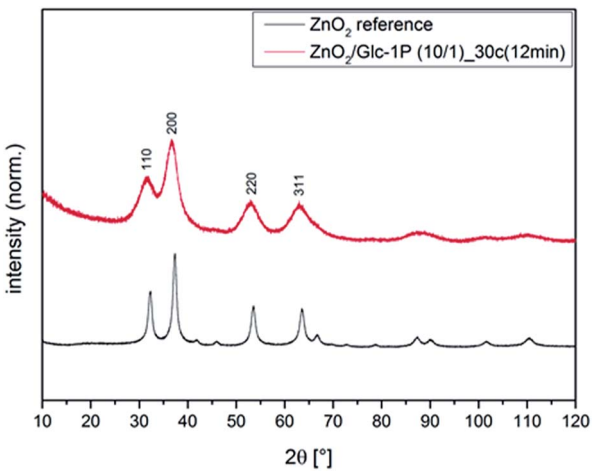

Fig. 2 Representative XRD measurement of biofunctionalized zinc peroxide nanoparticles in comparison to a zinc peroxide reference.

Further different reaction times and $Zn(ac)_2$: Glc-1P ratios influenced the sample compositions. Inductively coupled plasma atom emission spectroscopy (ICP-OES) measurements allowed the determination of the chemical composition (Table 1). The measurements were performed by introducing a dispersion of the nanoparticles to an ionized argon gas which caused a complete ionization of the sample. The resulting ions could be separated by their different mass to charge ratios and it was possible to quantify the concentration of the zinc ions (Zn^{2+}) depending on the intensity of the corresponding ion signal.[56] This enabled the determination of the zinc peroxide glucose-1-phosphate amounts in synthesized ZnO_2 nanoparticles. The experimental data presented in Table 1 indicate that the chemical composition of ZnO_2 nanoparticles is almost not changing with reaction time. This is in line with our expectations because same concentrations of reagents were used in these experiments. The ZnO_2 : Glc-1P ratios vary between 30.35/69.46 and 37.65/62.34 wt% what is an evidence that a relatively high amount of Glc-1P could be immobilized on the nanoparticle surface. Additionally, these data indicate that the synthesis was quite reproducible. It was also possible to observe a correlation between the initial $Zn(ac)_2$: Glc-1P ratios and the resulting sample compositions. The amount of Glc-1P in ZnO_2 nanoparticles decreased from 69.46 wt% (synthesis ratio 1/1) to 6.08 wt% (synthesis ratio 10/1) while the zinc peroxide sample amount increased from 30.53 wt% to 93.91 wt%. This behavior was in line with the expectations due to the fact that a higher initial synthesis amount of glucose-1-phosphate should result in more immobilized stabilizer molecules on the nanoparticle surface. The experimental XRD and ICP-OES data indicate that the structure and chemical composition of nanoparticles can be well controlled by the variation of synthesis parameters. In addition, ICP-OES proves that the

Table 1 Chemical compositions, nanoparticle diameter and crystallite sizes of zinc peroxide nanoparticles synthesized at different reaction times and $Zn(ac)_2$: Glc-1P ratios determined *via* ICP-OES, TEM and XRD

Sample	Pre./ stab. ratio	Sample composition [wt%/wt%]	Particle diameter [nm] (TEM)	Crystallite sizes [nm] (XRD)
ZnO_2/Glc-1P (1/1)_10c (4 min)	1/1	33.82/66.17	9.4 ± 5.2	3.3 ± 0.5
ZnO_2/Glc-1P (1/1)_20c (8 min)	1/1	37.65/62.34	6.3 ± 2.2	3.1 ± 0.4
ZnO_2/Glc-1P (1/1)_30c (12 min)	1/1	30.53/69.46	5.0 ± 1.5	3.3 ± 0.4
ZnO_2/Glc-1P (1/1)_40c (16 min)	1/1	35.60/64.39	6.3 ± 1.8	3.1 ± 0.3
ZnO_2/Glc-1P (2/1)_30c (12 min)	2/1	50.89/49.10	4.5 ± 1.2	2.3 ± 0.2
ZnO_2/Glc-1P (4/1)_30c (12 min)	4/1	73.61/26.38	4.2 ± 1.3	2.8 ± 0.1
ZnO_2/Glc-1P (6/1)_30c (12 min)	6/1	71.49/28.50	4.1 ± 1.4	2.8 ± 0.2
ZnO_2/Glc-1P (8/1)_30c (12 min)	8/1	83.47/16.52	4.8 ± 1.7	2.8 ± 0.1
ZnO_2/Glc-1P (10/1)_30c (12 min)	10/1	93.91/6.08	4.0 ± 1.2 + aggr.	2.7 ± 0.2

This journal is © The Royal Society of Chemistry 2017

Open Access Article. Published on 09 August 2017. Downloaded on 2/13/2026 8:44:47 AM.
This article is licensed under a Creative Commons Attribution 3.0 Unported Licence.

amount of glucose-1-phosphate on the nanoparticle surface can be flexibly adjusted by the initial concentrations of precursor in the reaction mixture.

TEM measurements revealed that small and uniform nanoparticles could be obtained for all synthesized samples. The average diameter and corresponding standard deviations were determined by measuring over 100 separate nanoparticles for each sample (Table 1, Fig. 3 (only representative samples; other images see ESI4†)). It could be shown that different reaction times (cycle numbers) influenced the nanoparticle diameter while different precursor : glucose-1-phosphate ratios had nearly no effect on the nanoparticle sizes. The nanoparticle diameter decreased from 9.4 ± 5.2 to 5.0 ± 1.5 nm by increasing the reaction time from 4 to 12 min (cycle number from 10 to 30). The decrease of the nanoparticle sizes can be explained by the longer exposition of the particles to the shear and impact forces inside the reaction chamber. A longer expositions means that the nanoparticles are more often exposed to abrasive effects inside the reaction chamber which decreased the particle sizes. The decrease of the standard deviation would support this assumption. An additional increase of the reaction time to 16 min (cycle number 40) resulted in an increase of the particle diameter to 6.3 ± 1.8 nm. This behavior can be explained by Oswald ripening taking place at the long reaction times.[57] Contrary nanoparticle sizes between 4.1 ± 1.4 nm and 4.8 ± 1.7 nm could be detected for the $Zn(ac)_2$/Glc-1P ratios 2/1, 4/1, 6/1 and 8/1 indicating no influence of the precursor : stabilizer ratio to the nanoparticle sizes. Only the 10/1 sample showed a divergent behavior. Some aggregates/agglomerates could be detected beside the small nanoparticles indicating that a stabilizer sample amount of 6.08 wt% was not sufficient to prevent the nanoparticles fully from aggregation/agglomeration. Furthermore the comparison to the crystallite size calculations indicated that the synthesized nanoparticles consisted most probably of two or three crystallites each. These data showed that glucose-1-phosphate seemed to be a very effective stabilizer for the synthesis in impinging jet reactor due to the fact that even a stabilizer sample amount of 16.52 wt% led to uniform and small nanoparticles with a diameter of 4.8 ± 1.7 nm. This good stabilizer property could be assigned to the hydrophilic glucose ring, which could introduce a quite steric stabilization to the nanoparticle surface.

3.2 Chemical composition of ZnO_2 nanoparticles surface

Previous studies showed that phosphate functions had a very high affinity to metal oxide surfaces which resulted in a good stabilization of different metal oxide particles like titanium dioxide, stannic dioxide or zinc peroxide.[47,58,59] This led to the assumption that the Glc-1P should strongly interact with the zinc peroxide surface *via* its phosphate function leading to a stabilization of the nanoparticles. Solid state ^{31}-phosporous nuclear magnetic resonance measurements (^{31}P-NMR) were performed to investigate binding of Glc-1P to the surface of zinc peroxide nanoparticles. One representative synthesized sample (ZnO_2/Glc-1P (1/1)_30c (12 min)) and the reference substance Glc-1P were measured and the comparison of the different ^{31}P-NMR signals enabled the enlightenment of the type of interaction between the Glc-1P and the nanoparticle surface (Fig. 4a).

The reference substance measurement showed one signal at −11.59 ppm, which could be assigned to the phosphor atom and several signals at −47.24, −29.52, 5.90, 24.49, 41.33, 59.27 and 76.33 ppm which were the corresponding side bands of the phosphor signal caused through the magic angle spinning (MAS) at 5 kHz. Additionally the signal at 0.87 ppm could be assigned to residues of the internal standard compound (ammonium phosphate) with its spinning side bands at −16.84, 18.38 and 33.66 ppm. It can be seen that the phosphate signal at −11.59 ppm was quite discrete (signal width 5.43 ppm) indicating that only one confirmation of the O–P–O bond angle of the phosphate function was present.[60] Contrary to this the ^{31}P-NMR spectra of the synthesized sample showed many differences. For example showed the sample spectra not only one but two signals for the phosphor atom at −14.59 and 6.08 ppm with the corresponding side bands at −69.01, 51.07, 32.52, 21.28, 38.60, 56.24 and 74.48 ppm. These two signals were broadened (signal widths: 17.63 and 18.02 ppm) compared to the reference signal indicating a change of the O–P–O bond angle and the presence of different binding sites and modes of the phosphate function which was caused through the interaction of the Glc-1P with the zinc peroxide surface.[60,61] Additionally an upfield

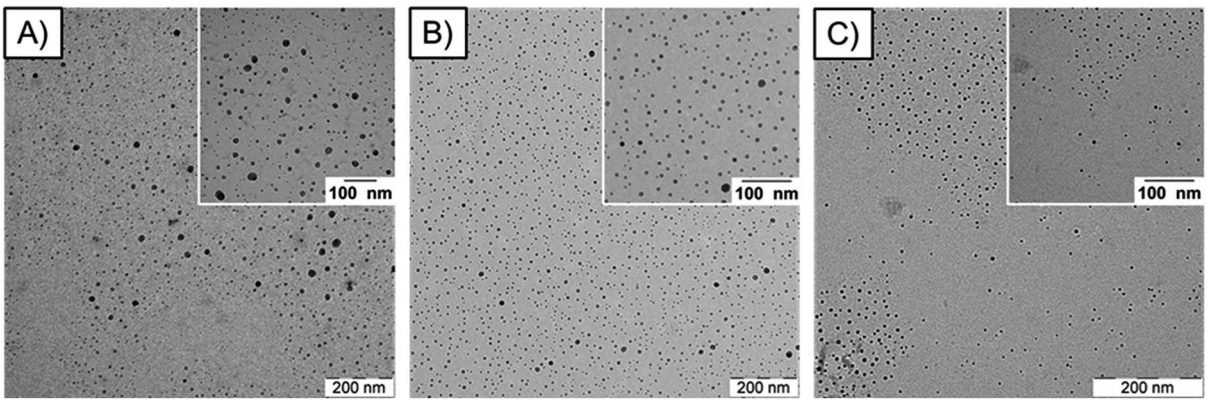

Fig. 3 TEM images of the representative ZnO_2/Glc-1P samples: (A) ZnO_2/Glc-1P (1/1)_10c (4 min), (B) ZnO_2/Glc-1P (1/1)_20c (8 min) and (C) ZnO_2/Glc-1P (1/1)_30c (12 min).

Open Access Article. Published on 09 August 2017. Downloaded on 2/13/2026 8:44:47 AM.
This article is licensed under a Creative Commons Attribution 3.0 Unported Licence.

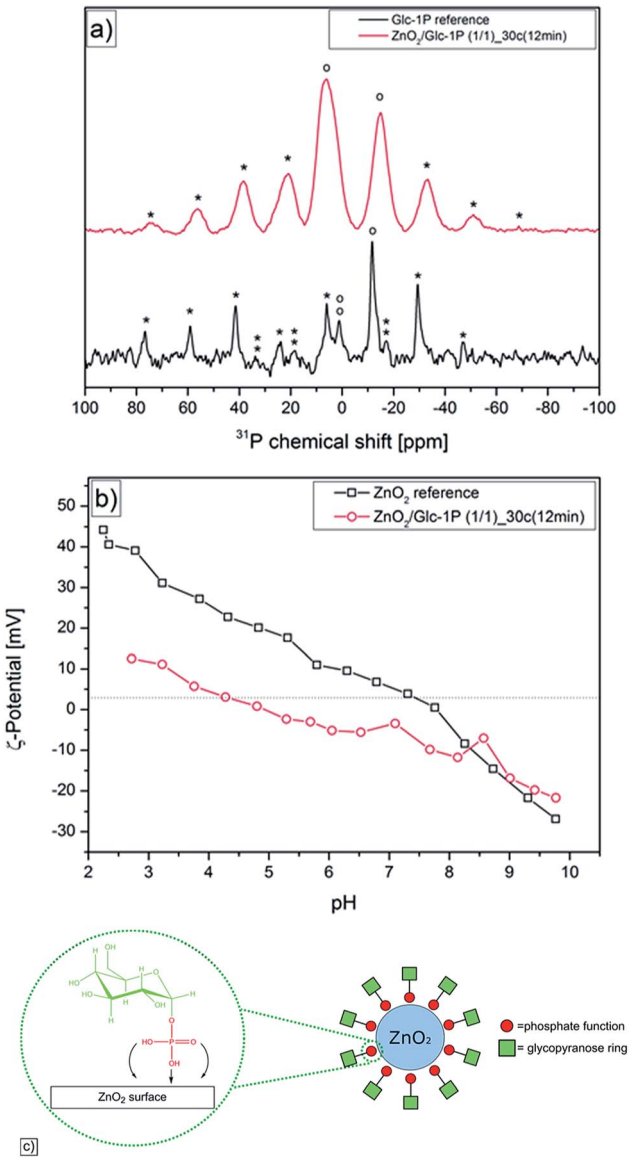

Fig. 4 ^{31}P solid state NMR spectra of ZnO_2/Glc-1P (1/1)_30c (12 min) and the reference substance Glc-1P with the phosphate signal (○), internal standard signal (○ ○) and their corresponding side bands (* and **) (a); pH dependent zeta-potential measurements of ZnO_2/Glc-1P (1/1)_30c (12 min) and the reference substance zinc peroxide (b); schematic illustration of the interaction of Glc-1P with the ZnO_2 nanoparticle surface (c).

shift (lower ppm) of −3.0 ppm and a downfield shift (higher ppm) of +17.6 ppm was observed for the two different phosphor signals compared to the one reference signal. Previous studies showed that an upfield shift is mostly caused through the chemisorption of phosphate ligands *via* the P–OH function on metal oxide surfaces resulting in mono-, bi- or trident bondings.[62] Considering the relatively low upfield shift of −3.0 ppm a mono dentate bonding of the Glc-1P on the nanoparticle surface is most likely. The strong downfield shift of +17.6 ppm can be explained through the interaction between the P=O function and hydroxyl functions present on the nanoparticle surface (physisorption).[62] This two different types of interaction are in good correlation to the broadening of the NMR signals mentioned above and proved clearly the binding of Glc-1P on the nanoparticle surface.

Additionally pH dependent zeta-potential measurements were performed to validate and support the assumptions made based on the ^{31}P solid-state NMR measurements (Fig. 4b). A modification of the zinc peroxide surface by the glucose-1-phosphate should result in a variation of the surface charge of the synthesized nanoparticles. The comparison with a reference measurement of unmodified zinc peroxide revealed that indeed differences occurred. The zeta-potential measurement showed for the zinc peroxide reference the typical ampholyte behavior with an isoelectric point at approximately pH = 8.00. This behavior is caused *via* the hydroxide functions present on the surface of unmodified zinc peroxide. The hydroxide functions were protonated in acidic media which resulted in a positive surface charge (44.52 mV), while they were deprotonated in basic media resulting in a negative surface charge (−27.28 mV).[63] Contrary the measurement of the modified nanoparticles showed a different behavior. Again an ampholyte progression could be observed but the isoelectric point was shifted to the pH value 4.88. Additionally a decrease of the surface charge could be observed. For example, difference in surface charge of approximately 30.00 mV at pH = 2.50 was observed, while at a pH value of 8.20 the difference between the modified nanoparticles and the reference zinc peroxide was nearly not existing. This divergent and approaching behavior can be explained through the glucose ring of the stabilizer. This contains four hydroxide functions, which can be protonated and deprotonated similar to the hydroxide functions of the non-modified zinc peroxide. But due to the modification of the nanoparticle surface and the steric demanding of the glucose ring a significant decrease of the accessible surface hydroxide functions was achieved in comparison to non-modified zinc peroxide. This decrease caused the lower surface charge in acidic and lightly basic media and explained the approaching of the two measured curves in stronger basic media.

3.3 Oxygen release properties of ZnO_2 nanoparticles

Beside the investigations of the sample compositions, the nanoparticle sizes, morphologies and surface properties, the oxygen release properties of the ZnO_2 nanoparticles were investigated. Previous studies showed that the oxygen release from ZnO_2 nanoparticles can be triggered by temperature increase or pH variation.[47] Due to the fact that the Glc-1P functionalized ZnO_2 nanoparticles can be potentially used for biomedical applications, we only investigated the pH triggered oxygen release in aqueous solutions. Zinc peroxide dissociates in aqueous acidic media into zinc ions (Zn^{2+}) and hydrogen peroxide (H_2O_2) while the hydrogen peroxide can be immediately converted into water and oxygen in presence of metal salts or metal oxide surfaces which are provided by the nanoparticles (Fig. 5c).[64,65] The quantifications of the pH induced oxygen releases of the different samples were done by time dependent measurements (approximately six days) *via* an optical oxygen sensor FDO®925 from WTW (functionality information are discussed in Section 2.3) (Fig. 5, Table 2).

This journal is © The Royal Society of Chemistry 2017

Open Access Article. Published on 09 August 2017. Downloaded on 2/13/2026 8:44:47 AM.
This article is licensed under a Creative Commons Attribution 3.0 Unported Licence.

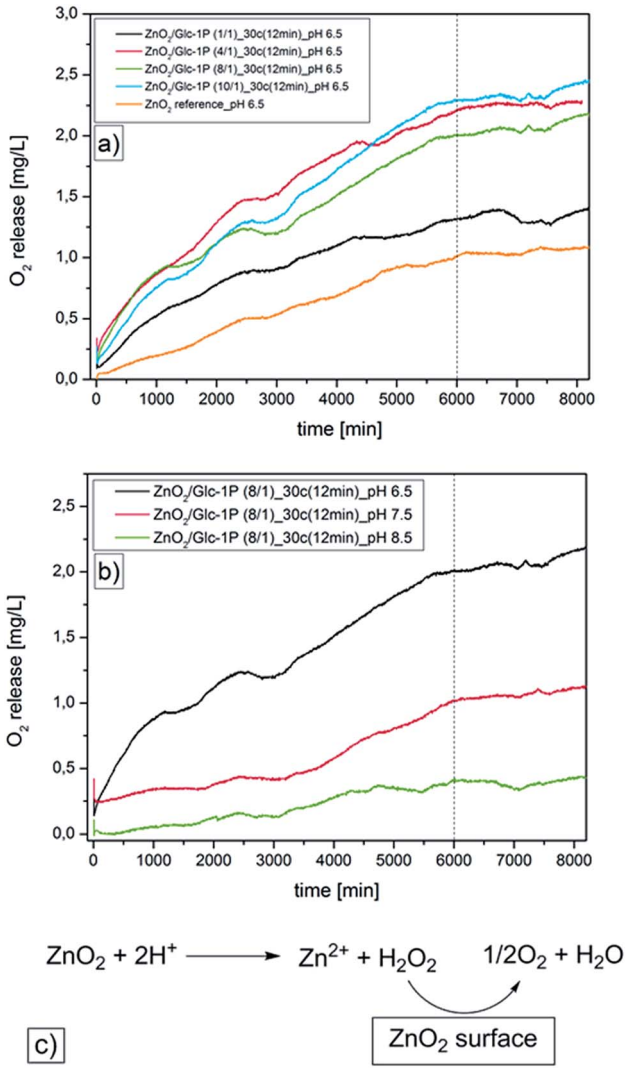

Fig. 5 Time dependent oxygen release measurements in aqueous media for different samples at constant pH value (a) and for one sample at different pH values (b); schematic illustration of the pH induced oxygen release from zinc peroxide (c).

Table 2 Amount of released oxygen from different ZnO_2 nanoparticle samples (measurements performed at $T = 23.0$ to 24.0 °C and ZnO_2 concentration in water $c = 1$ g L^{-1})

Sample	pH	Oxygen release [mg L^{-1}]
ZnO_2/Glc-1P (1/1)_30c (12 min)	6.5	1.38
ZnO_2/Glc-1P (4/1)_30c (12 min)	6.5	2.26
ZnO_2/Glc-1P (8/1)_30c (12 min)	6.5	2.06
ZnO_2/Glc-1P (10/1)_30c (12 min)	6.5	2.33
ZnO_2/Glc-1P (8/1)_30c (12 min)	7.5	1.05
ZnO_2/Glc-1P (8/1)_30c (12 min)	8.5	0.39
ZnO_2 reference	6.5	0.93

The measurements were carried out in degassed aqueous media under an inert argon atmosphere to prevent a distortion of the quantification through atmosphere oxygen. Additionally a water reference measurement was performed at identical measurement conditions and these data were used as a baseline. The measurements were carried out at different pH values (8.5, 7.5, 6.5) and at room temperature ($T = 23$ to 24 °C). The measurements showed for all samples a constant oxygen release for at least four days resulting in a saturation curve, which can be explained through the measurement setup. The measurement solutions were degassed and kept under an argon atmosphere to ensure that nearly no oxygen is present at the measurement start. Afterwards the nanoparticles released constantly oxygen which concentrated in the measurement solution until the nanoparticles became inactive which caused the plateau beginning after four days. The comparison with literature values proved that the plateau can only be caused through the nanoparticle deactivation due to the fact that the maximum concentration of dissolved oxygen in water was not reached at the end of the measurements (8.7 to 8.4 mg L^{-1} at 23 to 24 °C).[66] The measurements of the different samples at a constant pH value of 6.5 revealed that the amount of released oxygen was dependent on the sample compositions and the nanoparticle sizes (Fig. 5a). The amount of released oxygen increased with increasing zinc peroxide sample content and with decreasing nanoparticle diameter. For example sample ZnO_2/Glc-1P (1/1)_30c (12 min)_pH 6.5 released 1.38 mg L^{-1} oxygen while the sample ZnO_2/Glc-1P (10/1)_30c (12 min)_pH 6.5 already released 2.33 mg L^{-1}. This increase correlated with the corresponding zinc peroxide contents of 30.53 and 93.91 wt% as well with the nanoparticle diameter of 5.0 ± 1.5 and 4.0 ± 1.2 nm. Only the sample ZnO_2/Glc-1P (4/1)_30c (12 min)_pH 6.5 did not fit to this expectations. This sample showed a higher oxygen release of 2.26 mg L^{-1} compared to the sample ZnO_2/Glc-1P (8/1)_30c (12 min)_pH 6.5 (2.06 mg L^{-1}) despite its lower zinc peroxide content (73.61 wt%) compared to the 8/1 sample (83.47 wt%). The measurements showed also that all synthesized samples released more oxygen than the measured bulk reference substance (0.93 mg L^{-1}). Even the sample ZnO_2/Glc-1P (1/1)_30c (12 min)_pH 6.5 showed a higher activity despite it's relatively low zinc peroxide content of 30.53 wt%. These observations supported the assumption that smaller particles were capable of releasing more oxygen because of the larger surface area.

In addition to the influence of the sample composition and the particle size of ZnO_2 nanoparticles on the amount of released oxygen, the influence of different pH values was investigated. Different pH dependent measurements (pH = 8.5, 7.5, 6.5) of the same sample (ZnO_2/Glc-1P (8/1)_30c (12 min)) showed that with decreasing pH value the oxygen release increased (Fig. 5b). The amount of released oxygen increased constantly from 0.39 to 1.05 and 2.06 mg L^{-1} with changing pH value from 8.5 to 7.5 and 6.5. This observations were in line with the expectations due to the fact that a slightly acidic environment accelerates the oxygen release by faster decomposition of the zinc peroxide nanoparticles.[64,65]

3.4 Interaction of ZnO_2 nanoparticles with proteins

After demonstration that the glucose-1-phosphate could be immobilized on the nanoparticle surface the recognition of the

Open Access Article. Published on 09 August 2017. Downloaded on 2/13/2026 8:44:47 AM.
This article is licensed under a Creative Commons Attribution 3.0 Unported Licence.

glucose molecule by the lectin Concanavalin A (ConA) was investigated *via* fluorescence measurements. Lectins are structurally diverse carbohydrate-binding proteins of non-immune origin. Most of these lectins possess two or more sugar binding sites and can agglutinate cells and/or precipitate complex carbohydrate conjugates.[67,68] They are normally located in the glycocalyx, a carbohydrate cell coating consisting of membrane, glycoproteins, glycolipids and glycosaminoglycans and are responsible for cell–cell interactions by combining with complementary carbohydrates on opposing cells.[69–71]

For this study the lectin Concanavalin A (ConA) was used to show that the synthesized nanoparticles indeed interact specifically with biomolecules through the surface located glucose function. ConA is a lectin, which interacts specifically with the α forms of mannose and glucose and can be found in plants, animals and microorganisms.[68,72,73] The protein consists of four identical subunits with a molecular weight of approximately 27 000 for each monomeric unit.[74,75] ConA subunit interactions are dependent on pH. At pH values between 2.0 and 5.5 ConA consists of two non covalently bound subunits building a dimer, whereas at pH values above 5.5 a tetramer with a molecular weight of 110 000 Da is formed.[76,77] The interactions between the subunits contain mostly of hydrogen and salt bridge bonds explaining the pH dependence.[75] The subunit carbohydrate binding sites of ConA facilitate mostly hydrogen bonds to the oxygen atoms of glucose or mannose through the amino acid residues Arg228, Asn14, Asp208, Tyr100 and Leu99.[78] During this interaction the position of the oxygen atoms of the sugar molecules is crucial for the strength of the resulting bonding. Previous studies showed that ConA establishes in total eleven hydrogen bonds to methyl-α-D-mannopyranoside but especially three bonds showed an increased stability due to nearly linear bond angles and short bond lengths caused through the O-atom-positions. Beside the hydrogen bonds hydrophobic interactions take also part in the specific interaction of ConA and glucose or mannose molecules. It was shown that the aromatic ring of Tyr12 interacts with two C atoms of the pyranose ring resulting in a stabilization of the binding site.[78] These specifications made the ConA a suitable choice to investigate the binding properties of the synthesized and functionalized zinc peroxide nanoparticles.

Two different types of fluorescent measurements were performed to investigate the specific interactions between the ConA and the functionalized nanoparticles (Fig. 6). First, the quantification of the interactions was investigated for different synthesized ZnO_2 samples followed by an inhibition measurement of one selected sample. The quantification of the immobilized ConA on the nanoparticle surface was achieved through it's labeling with the fluorescent dye Oregon Green. Additionally to these measurements a reference measurement (ZnO_2-ref) of comparable zinc peroxide nanoparticles ($d = 6.1 \pm 2.9$ nm) stabilized with the organic molecule dioctyl sulfosuccinate (AOT) was performed too (characterization details see ESI5 and 6†). The surface charge of these particles was nearly neutral (−2.0 mV) at selected measurement conditions (similar to Glc-1P stabilized particles), but contrary these particles should not show any binding of ConA due to absence of glucose or mannose molecules on the nanoparticle surface.

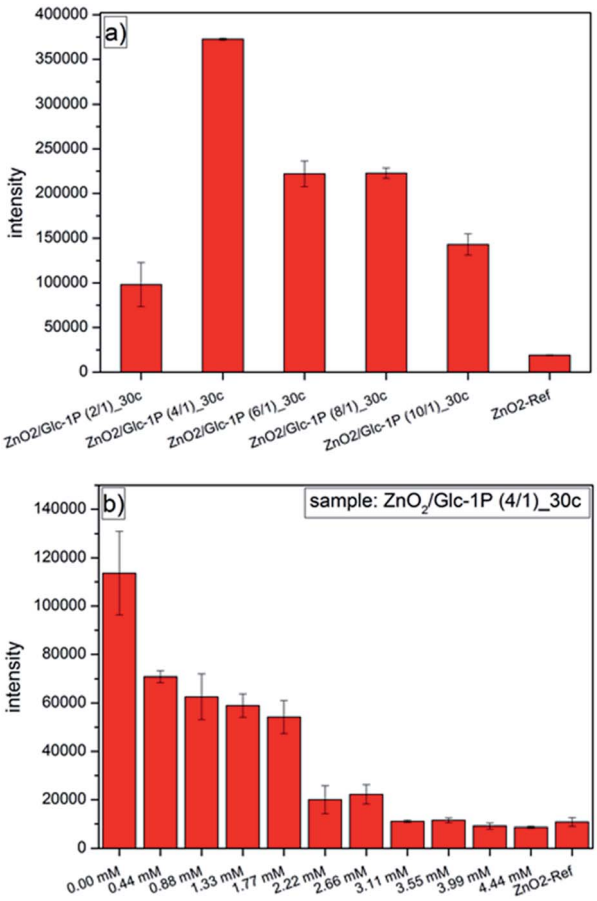

Fig. 6 Fluorescence measurements for the investigation of the ConA binding to ZnO_2 surface: for the different synthesized samples (a); inhibition measurement for one sample at different mannose concentrations (b).

The fluorescence measurements for the different synthesized samples (Fig. 6a) showed clearly a dependence of the ConA binding properties of the nanoparticles to the different sample compositions. All Glc-1P functionalized ZnO_2 nanoparticles showed a significant higher fluorescence compared to the reference nanoparticles stabilized with the surfactant AOT. The reference measurement showed only a minor fluorescence caused by non-specifically bound ConA.[79] The significantly higher fluorescence of the other samples can only be explained through a higher amount of immobilized ConA indicating the specific interaction of the ConA with the accessible glucose rings on the nanoparticles surface.[78] Additionally the interaction between the nanoparticles and the ConA was dependent on the sample compositions but did not show the expected trend. A higher sample content of Glc-1P should result in a better immobilization of the ConA and subsequently in a higher fluorescence but the sample ZnO_2/Glc-1P (2/1)_30c (12 min) with the highest Glc-1P amount of 49.10 wt% showed the lowest fluorescence of the Glc-1P functionalized nanoparticles. In contrast to that the sample ZnO_2/Glc-1P (4/1)_30c (12 min) (Glc-1P amount = 26.38 wt%) showed the highest fluorescence followed by a continuously decrease in fluorescence (fewer immobilization of ConA) with

 This journal is © The Royal Society of Chemistry 2017

Open Access Article. Published on 09 August 2017. Downloaded on 2/13/2026 8:44:47 AM.
This article is licensed under a Creative Commons Attribution 3.0 Unported Licence.

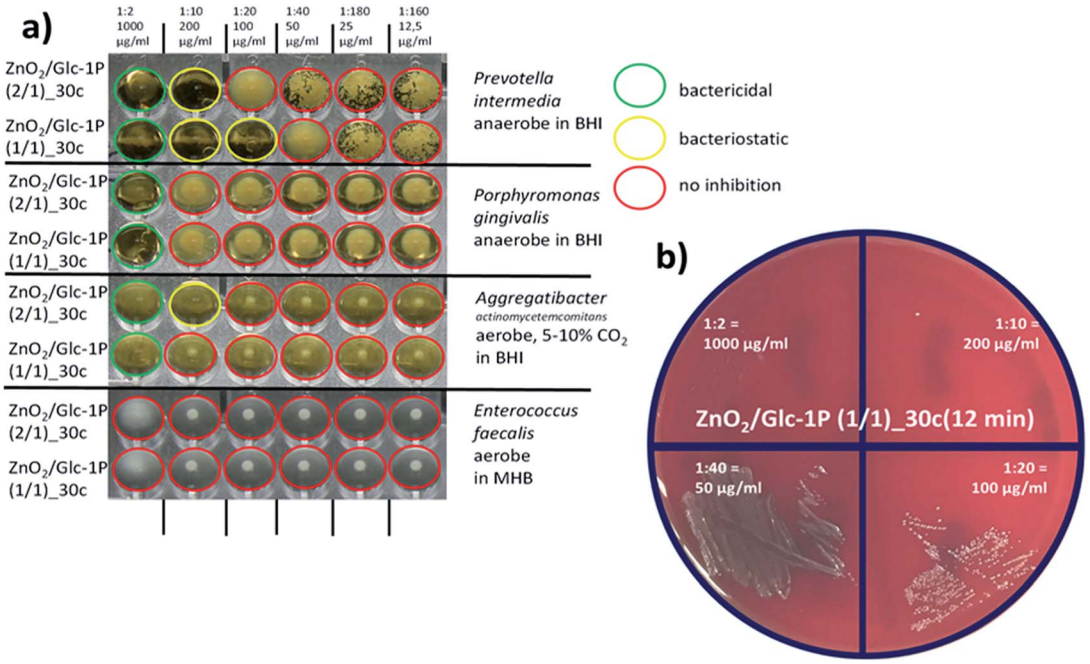

Fig. 7 Antimicrobial properties of zinc peroxide nanoparticles ZnO_2/Glc-1P (2/1)_30c (12 min) and ZnO_2/Glc-1P (1/1)_30c (12 min): (a) microbroth dilution testing to determine the minimal inhibitory concentration (MIC) of different zinc peroxide nanoparticles and concentrations by serial dilutions 1 : 2 to 1 : 160 (corresponding to 1000–12.5 µg mL^{-1}) in microtiter plates. Test-strains, atmospheric conditions of growth and broth medium (BHI Brain Heart Infusion Broth pH 7.4 ± 0.2; MHB Mueller Hinton Broth, pH 7.4 ± 0.2) are indicated and the circles in different colors indicate complete killing (bactericidal), inhibition (bacteriostatic) or no definite inhibitory effect. (b) Determination and proof of the minimal bactericidal concentration (MBC) of ZnO_2/Glc-1P (1/1)_30c (12 min) and *Prevotella intermedia* as test strain. Striking of 30 µL suspension from the microtiter-wells shown in (a) on Trypticase Soy Agar with blood and incubation overnight in appropriate atmosphere disclosed the killing effect of zinc peroxide nanoparticles. In this case, ZnO_2/Glc-1P (1/1)_30c (12 min) in a concentration of 1000 µg mL^{-1} killed all bacterial cells whereas in a concentration of 200 µg mL^{-1} (dilution 1 : 10) a single cell (better: colony forming unit) could still survive. Because of the clear microbial inhibition and killing observed with ZnO_2/Glc-1P (1/1)_30c (12 min) of *P. intermedia* and because of the lack of any other appropriate and comparable substance, this combination was used as a positive control further on.

decreasing Glc-1P content for the other samples. An explanation for lower binding of ConA to the ZnO_2/Glc-1P (2/1)_30c (12 min) sample could be that the accessibility of the glucose rings was inhibited due to the high amount of stabilizer (higher packing density) which could cause a different orientation of the Glc-1P molecules on the nanoparticle surface compared to the other samples. Similar results were achieved for the stabilization of gold nanoparticles with different carbohydrates. The investigations showed that carbohydrates with longer spacer units provided a better immobilization of ConA due to the better accessibility of the mannose rings.[80]

To support the assumption that the ConA specifically interacted with the glucose ring of the Glc-1P additionally one inhibition measurement was performed for the sample ZnO_2/Glc-1P (4/1)_30c (12 min) (Fig. 6b). The difference to the previous measurements was that different amounts of mannose were added to the measurement solution before the addition of the ConA. Through the higher specific affinity of the ConA to the mannose than to the glucose a steady decrease of the ConA binding to the nanoparticles should be observed with increasing mannose concentration. The higher affinity of the mannose to the ConA is mostly based on the geometrical position of it's hydroxyl group oxygen atom. For example are eighteen atoms within the ConA binding pocket in a range of 4 Å to this oxygen atom while for the glucose hydroxyl group oxygen atom only five atoms are in the same range. This results in the formation of more extensive van der Waals forces for the mannose causing a higher affinity.[81,82] The fluorescence measurements showed exactly this behavior. The fluorescence of the particles decreased with increasing mannose concentration showing that fewer ConA molecules were immobilized on the nanoparticle surface. A critical point was reached at a mannose concentration of 2.22 mM at which the fluorescence decreased strongly. After this point the Glc-1P functionalized nanoparticles showed nearly the same fluorescence like the reference nanoparticles indicating that no ConA was immobilized specifically after this point anymore and that it reacted with the mannose and was washed away during the cleaning process. These measurements showed that the functionalization of the zinc peroxide nanoparticles with Glc-1P lead to specific interactions with ConA and represents a proof of principal for the application of the nanoparticles in biological systems.

3.5 Antibacterial properties of ZnO_2 nanoparticles

The microbiological results are presented in Fig. 7 for the two most active zinc peroxide nanoparticles tested so far, ZnO_2/Glc-1P (2/1)_30c (12 min) and ZnO_2/Glc-1P (1/1)_30c (12 min).

Open Access Article. Published on 09 August 2017. Downloaded on 2/13/2026 8:44:47 AM. This article is licensed under a Creative Commons Attribution 3.0 Unported Licence.

Susceptibility to both nanoparticles was not observed for the robust and aerotolerant Gram-positive species *Enterococcus faecalis*. *Aggregatibacter actinomycetemcomitans* was tested with a minimal inhibitory concentration (MIC) of 200 μg mL^{-1} against ZnO_2/Glc-1P (2/1)_30c (12 min) and 1000 μg mL^{-1} against ZnO_2/Glc-1P (1/1)_30c (12 min). *Porphyromonas gingivalis* was tested with a minimal inhibitory concentration (MIC) of 1000 μg mL^{-1} against both nanoparticles ZnO_2/Glc-1P (2/1)_30c (12 min) and ZnO_2/Glc-1P (1/1)_30c (12 min). The most susceptible species was found to be *Prevotella intermedia*, which was tested with a minimal inhibitory concentration (MIC) of 200 μg mL^{-1} against ZnO_2/Glc-1P (2/1)_30c (12 min) and even down to 100 μg mL^{-1} against ZnO_2/Glc-1P (1/1)_30c (12 min), the latter combination used as a positive control further on. The minimal bactericidal concentration (MBC) for both zinc peroxide nanoparticles was found to be 1000 μg mL^{-1} for all fastidious bacterial species but not for *E. faecalis*.

These results are in line with the expectation, that the more aerotolerant (resistant to ROS) a bacterial species is, the more it is tolerant to oxygen releasing nanoparticles. Thus, the most susceptible species can be found among obligate anaerobe species such as *P. gingivalis* and *P. intermedia*. Interestingly, *P. intermedia*, known as slightly more aerotolerant than *P. gingivalis*, was more susceptible (MIC 100–200 μg mL^{-1}). This might be due to a higher initial inoculum chosen for *P. gingivalis* (10^5 instead of otherwise 10^4 cells) to guarantee the principal growth of this very fastidious organism. Also unexpectedly, *P. intermedia* was slightly more susceptible against ZnO_2/Glc-1P (1/1)_30c (12 min) with a MIC of 100 μg mL^{-1} than ZnO_2/Glc-1P (2/1)_30c (12 min) with a MIC of 200 μg mL^{-1}. This could be evidence for the fact that adherence mediated by the Glc-1P outer layer plays a very important role in the biological activity of the composed nanoparticles as the Glc-1P concentration is 69.46 wt% *versus* 49.10 wt% and thus 41.4% higher (Table 1). However, this finding has to be verified with additional obligate anaerobic (both Gram-negative and -positive) bacterial species and further ZnO_2/Glc-1P samples with a varying composition. The antimicrobial tests should also be repeated with different pH values as lower pH increases oxygen release (Fig. 5b). However, as a pH of 7.4 ± 0.4 is optimal for most microorganisms the physiological range for testing is rather limited.

4 Conclusions

In this study we report facile synthesis route to obtain ultrasmall and uniform biofunctionalized glucose-1-phosphate (Glc-1P)-coated zinc peroxide (ZnO_2) nanoparticles. The synthesized nanoparticles revealed diameters between 4.0 ± 1.2 nm and 9.4 ± 5.2 nm depending on different reaction time and initial GLc-1P concentration. It could be shown *via* solid state ^{31}-phosporous nuclear magnetic resonance measurements (^{31}P-NMR) and pH dependent zeta-potential measurements that glucose-1-phosphate (Glc-1P) interacted with the nanoparticle surface *via* its phosphate function through chemi- and physisorption forming monodentate bonds and hydrogen bonds with ZnO_2 surface. This specific interaction, in combination with the special reaction system setup ensured formation of ultrasmall, monodisperse zinc peroxide nanoparticles with tunable size and controlled amount of surface-anchored Glc-1P. Fluorescence measurements showed a specific interaction between the lectin Concanavalin A (ConA) and Glc-1P attached to the nanoparticles surface. Time dependent measurements revealed that the ZnO_2 nanoparticles release different amounts of oxygen depending on the sample composition and the pH value of the aqueous solution. It could be shown that nanoparticles released oxygen up to four days and that a slightly acidic environment can accelerate the oxygen release. Antimicrobial tests (determination of MIC and MBC at 37 °C and pH 7.4 ± 0.2) performed with four bacterial species exhibiting different susceptibility to oxygen confirmed the antimicrobial activity of ZnO_2 nanoparticles.

Acknowledgements

Prof. Dan Demco is acknowledged for performing the solid state ^{31}-phosporous nuclear magnetic resonance measurements. We thank Beate Melzer-Krick for her excellent technical assistance. This study was supported by The German Research Community (Deutsche Forschungsgemeinschaft, DFG) *via* Exploratory Research Space (ERS), RWTH Aachen University (grant number: Dean's Seed Fund 2016-Zukunfskonzept II). This work was performed in part at the Center for Chemical Polymer Technology CPT, which is supported by the EU and the federal state of North Rhine-Westphalia (Grant No. EFRE 30 00 883 02). AP thanks VolkswagenStiftung for financial support.

Notes and references

1 J. M. A. Blair, M. A. Webber, A. J. Baylay, D. O. Ogbolu and L. J. V. Piddock, *Nat. Rev. Microbiol.*, 2015, **13**, 42–51.
2 E. Marti, E. Variatza and J. L. Balcazar, *Trends Microbiol.*, 2014, **22**, 36–41.
3 M. N. Alekshun and S. B. Levy, *Cell*, 2007, **128**, 1037–1050.
4 A. Giedraitienė, A. Vitkauskienė, R. Naginienė and A. Pavilonis, *Medicina*, 2011, **47**, 137–146.
5 L. Fernandez and E. W. Hancock, *Clin. Microbiol. Rev.*, 2012, **25**, 661–681.
6 L. J. V. Piddock, *Clin. Microbiol. Rev.*, 2006, **19**, 382–402.
7 G. De Pascale and G. D. Wright, *ChemBioChem*, 2010, **11**, 1325–1334.
8 R. M. Donlan, *Emerging Infect. Dis.*, 2002, **8**, 881–890.
9 K. Lewis, *Antimicrob. Agents Chemother.*, 2001, **45**, 999–1007.
10 R. M. Donlan and J. W. Costerton, *Clin. Microbiol. Rev.*, 2002, **15**, 167–193.
11 R. Patel, *Clin. Orthop. Relat. Res.*, 2005, **437**, 41–47.
12 W. M. Dunne, *Clin. Microbiol. Rev.*, 2002, **15**, 155–166.
13 K. Driffield, K. Miller, J. M. Bostock, A. J. O'neill and I. Chopra, *J. Antimicrob. Chemother.*, 2008, **61**, 1053–1056.
14 S. Molin and T. Tolker-Nielsen, *Curr. Opin. Biotechnol.*, 2003, **14**, 255–261.
15 B. M. Peters, M. E. Shirtliff and M. A. Jabra-Rizk, *PLoS Pathog.*, 2010, **6**, 4–7.
16 L. Good, *Methods Mol. Biol.*, 2002, **208**, 237–248.

 This journal is © The Royal Society of Chemistry 2017

Open Access Article. Published on 09 August 2017. Downloaded on 2/13/2026 8:44:47 AM. This article is licensed under a Creative Commons Attribution 3.0 Unported Licence.

17 N. K. Sahu, G. Shilakari, A. Nayak and D. V. Kohli, *Curr. Pharm. Biotechnol.*, 2007, **8**, 291–304.
18 P. Gilbert and L. E. Moore, *J. Appl. Microbiol.*, 2005, **99**, 703–715.
19 M. Kather, M. Skischus, P. Kandt, A. Pich, G. Conrads and S. Neuss, *Angew. Chem., Int. Ed.*, 2017, **56**, 1–7.
20 B. Ramalingam, T. Parandhaman and S. K. Das, *ACS Appl. Mater. Interfaces*, 2016, **8**, 4963–4976.
21 L. Rizzello and P. P. Pompa, *Chem. Soc. Rev.*, 2014, **43**, 1501–1518.
22 S. Chernousova and M. Epple, *Angew. Chem., Int. Ed.*, 2013, **52**, 1636–1653.
23 O. Bondarenko, A. Ivask, A. Käkinen, I. Kurvet and A. Kahru, *PLoS One*, 2013, **8**, e64060–e64072.
24 W. R. Li, X. B. Xie, Q. S. Shi, H. Y. Zeng, Y. S. Ou-Yang and Y. Ben Chen, *Appl. Microbiol. Biotechnol.*, 2010, **85**, 1115–1122.
25 E. Amato, Y. a. Diaz-Fernandez, A. Taglietti, P. Pallavicini, L. Pasotti, L. Cucca, C. Milanese, P. Grisoli, C. Dacarro, J. M. Fernandez-Hechavarria and V. Necchi, *Langmuir*, 2011, **27**, 9165–9173.
26 C. Carlson, S. M. Hussein, A. M. Schrand, L. K. Braydich-Stolle, K. L. Hess, R. L. Jones and J. J. Schlager, *J. Phys. Chem. B*, 2008, **112**, 13608–13619.
27 T. Tian, X. Shi, L. Cheng, Y. Luo, Z. Dong, H. Gong, L. Xu, Z. Zhong, R. Peng and Z. Liu, *ACS Appl. Mater. Interfaces*, 2014, **6**, 8542–8548.
28 J. Tang, Q. Chen, L. Xu, S. Zhang, L. Feng, L. Cheng, H. Xu and Z. Liu, *ACS Appl. Mater. Interfaces*, 2013, **5**, 3867–3874.
29 W.-P. Xu, L.-C. Zhang, J.-P. Li, Y. Lu, H.-H. Li, Y.-N. Ma, W.-D. Wang and S.-H. Yu, *J. Mater. Chem.*, 2011, **21**, 4593.
30 X. Shi, H. Gong, Y. Li, C. Wang, L. Cheng and Z. Liu, *Biomaterials*, 2013, **34**, 4786–4793.
31 K. Yang, L. Hu, X. Ma, S. Ye, L. Cheng, X. Shi, C. Li, Y. Li and Z. Liu, *Adv. Mater.*, 2012, **24**, 1868–1872.
32 K. Yang, S. Zhang, G. Zhang, X. Sun, S. T. Lee and Z. Liu, *Nano Lett.*, 2010, **10**, 3318–3323.
33 R. Kurapati, M. Vaidyanathan and A. M. Raichur, *RSC Adv.*, 2016, **6**, 39852–39860.
34 L. Zhang, Y. Jiang, Y. Ding, M. Povey and D. York, *J. Nanopart. Res.*, 2007, **9**, 479–489.
35 X. Peng, S. Palma, N. S. Fisher and S. S. Wong, *Aquat. Toxicol.*, 2011, **102**, 186–196.
36 N. Padmavathy and R. Vijayaraghavan, *Sci. Technol. Adv. Mater.*, 2008, **9**, 35004.
37 N. Hao, K. W. Jayawardana, X. Chen and M. Yan, *ACS Appl. Mater. Interfaces*, 2015, **7**, 1040–1045.
38 D. L. Clemens, B. Y. Lee, M. Xue, C. R. Thomas, H. Meng, D. Ferris, A. E. Nel, J. I. Zink and M. A. Horwitz, *Antimicrob. Agents Chemother.*, 2012, **56**, 2535–2545.
39 J. S. Dickson, M. Koohmaraie and R. L. Hruska, *Appl. Environ. Microbiol.*, 1989, **55**, 832–836.
40 K. H. Muhvich, M. K. Park, R. A. M. Myers and L. Marzella, *Antimicrob. Agents Chemother.*, 1989, **33**, 1526–1530.
41 J. T. Mader, G. L. Brown, J. C. Guckian, C. H. Wells and J. A. Reinarz, *J. Infect. Dis.*, 1980, **142**, 915–922.
42 T. K. Hunt, M. Linsey, H. Grislis, M. Sonne and E. Jawetz, *Ann. Surg.*, 1975, **181**, 35–39.
43 D. R. Knighton, B. Halliday and T. K. Hunt, *Arch. Surg.*, 1986, **121**, 191–195.
44 D. R. Knighton, V. D. Fiegel, T. Halverson, S. Schneider, T. Brown and C. L. Wells, *Arch. Surg.*, 1990, **125**, 97–100.
45 M. Cimşit, G. Uzun and S. Yildiz, *Expert Rev. Anti-Infect. Ther.*, 2009, **7**, 1015–1026.
46 M. K. Park, K. H. Muhvich, R. A. M. Myers and L. Marzella, *Hyperbaric Medicine Practice*, ed. H. T. Whelan, Best Publishing, Flagstaff, 2004.
47 C. Bergs, P. Simon, Y. Prots and A. Pich, *RSC Adv.*, 2016, **6**, 84777–84786.
48 H. Bai and X. Liu, *Mater. Lett.*, 2010, **64**, 341–343.
49 Q. A. Drmosh, M. A. Gondal, Z. H. Yamani and T. A. Saleh, *Appl. Surf. Sci.*, 2010, **256**, 4661–4666.
50 M. Sun, W. Hao, C. Wang and T. Wang, *Chem. Phys. Lett.*, 2007, **443**, 342–346.
51 D. Flanagan, *J. Oral. Implantol.*, 2017, **43**, 8–11.
52 H. M. S. Goh, M. H. A. Yong, K. K. L. Chong and K. A. Kline, *Virulence*, 2017, 1–38.
53 A. D. Pye, D. E. Lockhart, M. P. Dawson, C. A. Murray and A. J. Smith, *J. Hosp. Infect.*, 2009, **72**, 104–110.
54 L. F. Zhunag, R. M. Watt, N. Mattheos, M. S. Si, H. C. Lai and N. P. Lang, *Clin. Oral Implants Res.*, 2016, 13–21.
55 P. M. Aneesh, K. A. Vanaja and M. K. Jayaraj, *Nanophotonic Mater. IV*, 2007, vol. 6639, p. 66390J.
56 V. Fassel, *Science*, 1978, **202**, 183–191.
57 M. Köhler, in *Chemische Technik: Prozesse und Produkte*, WILEY-VCH Verlag GmbH & Co. KGaA, Weinheim, 2004, pp. 821–905.
58 N. Adden, L. Gamble, D. Castner, A. Hoffmann, G. Gross and H. Menzel, *Langmuir*, 2006, **22**, 8197–8204.
59 G. P. Holland, R. Sharma, J. O. Agola, S. Amin, V. C. Solomon, P. Singh, D. a. Buttry and J. L. Yarger, *Chem. Mater.*, 2007, **19**, 2519–2526.
60 W. Gao, L. Dickinson, C. Grozinger, F. G. Morin and L. Reven, *Langmuir*, 1996, **12**, 6429–6435.
61 W. Gao, L. Dickinson, C. Grozinger, F. F. G. Morin and L. Reven, *Langmuir*, 1997, **13**, 115–118.
62 J. P. Osegovic and R. S. Drago, *J. Phys. Chem. B*, 2000, **104**, 147–154.
63 S. Liufu, H. Xiao and Y. Li, *Powder Technol.*, 2004, **145**, 20–24.
64 Y. Wolanov, P. V. Prikhodchenko, A. G. Medvedev, R. Pedahzur and O. Lev, *Environ. Sci. Technol.*, 2013, **47**(15), 8769–8774.
65 E. H. Bawn, *Catalytic decomposition of hydrogen peroxide on differnt metals*, 1935.
66 R. F. Weiss, *Deep-Sea Res. Oceanogr. Abstr.*, 1970, **17**, 721–735.
67 I. Damjanov, *Lab. Invest.*, 1987, **57**, 5–20.
68 I. J. Goldtein and R. D. Poretzt, *The Lectins: Properties, Functions, and Applications in Biology and Medicine*, 1986.
69 R. Schauer, C. Fischer, H. Lee, B. Ruch and S. Kelm, *Lectins and Glycoconjugates in Oncology*, 1988.
70 B. K. Brandley and R. L. Schnaar, *J. Leukocyte Biol.*, 1986, **40**, 97–111.

Open Access Article. Published on 09 August 2017. Downloaded on 2/13/2026 8:44:47 AM.
This article is licensed under a Creative Commons Attribution 3.0 Unported Licence.

71 F. L. Harrison and C. J. Chesterton, *FEBS Lett.*, 1980, **122**, 157–165.
72 R. Mody, S. H. a. Joshi and W. Chaney, *J. Pharmacol. Toxicol. Methods*, 1995, **33**, 1–10.
73 H. Lis and N. Sharon, *Annu. Rev. Biochem.*, 1986, **55**, 35–67.
74 K. Hardman and C. Ainsworth, *Biochemistry*, 1972, **11**, 4910–4919.
75 G. Reeke, J. Becker and G. Edelman, *J. Biol. Chem.*, 1975, **250**, 1525–1547.
76 J. L. Wang, B. a Cunningham and G. M. Edelman, *Proc. Natl. Acad. Sci. U. S. A.*, 1971, **68**, 1130–1134.
77 B. B. L. Agrawal and I. J. Goldtein, *Biochim. Biophys. Acta*, 1967, **147**, 262–271.
78 T. Li, H. B. Lee and K. Park, *J. Biomater. Sci., Polym. Ed.*, 1998, **9**, 327–344.
79 A. Salvati, C. Åberg, K. A. Dawson and M. P. Monopoli, *Nat. Nanotechnol.*, 2012, **7**, 779–786.
80 C. C. Lin, Y. C. Yeh, C. Y. Yang, G. F. Chen, Y. C. Chen, Y. C. Wu and C. C. Chen, *Chem. Commun.*, 2003, **9**, 2920–2921.
81 P. Rouge and B. Sousa-Cavada, *Plant Sci. Lett.*, 1984, **37**, 21–27.
82 R. D. Poretzt and I. J. Goldstein, *Biochemistry*, 1970, **9**, 2890–2896.

This journal is © The Royal Society of Chemistry 2017